Vacuum 155 (2018) 559–565

Contents lists available at ScienceDirect

Vacuum

journal homepage: www.elsevier.com/locate/vacuum

Linear magnetron HiPIMS high deposition rate magnet pack

Jake McLain*, Priya Raman, Dhruval Patel, Randall Spreadbury, Jan Uhlig, Ivan Shchelkanov, D.N. Ruzic

Department of Nuclear, Plasma, and Radiological Engineering, University of Illinois at Urbana-Champaign, IL, USA

ABSTRACT

High Power Impulse Magnetron Sputtering (HiPIMS) or High Power Pulsed Magnetron Sputtering (HPPMS) is a promising magnetron sputtering technique for ionized physical vapor deposition (iPVD), with industrial implementation hindered by low deposition rates in non-reactive HiPIMS. Because HiPIMS is currently of low interest in high volume manufacturing where deposition rates should be high, there is a demand for a solution to the low deposition rate problem, scalable to any desired length. To increase the deposition rate, a magnet pack behind a linear magnetron target is altered, and the new magnetic field is designed to allow for an increased ion flux to the substrate. The modeled magnet pack is manufactured and named the linear tripack magnet pack. Deposition rate is discussed for both DCMS and HiPIMS, using both a standard linear magnet pack and the linear tripack magnet pack in non-reactive HiPIMS. Observed deposition rates for the linear tripack magnet pack are found to be equal to or greater than the DC standard magnet pack at 1.5 kW and copper ionized flux fraction measurements were found to be as high as 35% at the substrate for the linear tripack magnet pack at 3.2 kW. Electron temperature and electron density measurements are taken and discussed.

1. Introduction

High Power Impulse Magnetron Sputtering (HiPIMS) is an ionized physical vapor deposition (iPVD) technique that applies high power pulses to the magnetron sputtering target at low duty cycles. The instantaneous applied power densities can be reach tens of kilowatts per square centimeter, while the time averaged power density remains comparable to DC magnetron sputtering (DCMS) power densities. In a HiPIMS discharge, the electron densities in the near target plasma can reach values up to three orders of magnitude greater than in DCMS. This significantly increases the ionization rate of the sputtered material, thereby increasing the ion flux to the substrate [1]. This intrinsically high ion flux allows for the deposition of films and coatings with higher quality and density, as much as an increase of 30%, when compared with DCMS [2,3]. Although the high ion flux produces desirable film traits, the HiPIMS mode suffers from the major drawback of typically lower deposition rates than DCMS in non-reactive HiPIMS, due to sputtered ions returning back to the target [4]. For copper targets, this has previously been reported to constitute a drop in deposition rate in the range of 30–70% [3,5,6].

The issue of low HiPIMS deposition rates is not a simply solved one, and there are many ways to mitigate it. One approach that has been investigated is to decrease the magnetic field strength, which has been shown to provide an increase in deposition rate from 4.5 to 6 times a standard magnet pack [7,8]. Alternatively, the magnetic field topology has shown to effect the deposition rate in Raman et al., where a symmetric 10.2 cm circular magnet pack with multiple confinement regions increased deposition rate [9,10]. The deposition rate is increased by creating a magnet pack with routes for controlled electron loss, causing an increase in ion deposition by both ambipolar diffusion, and an expanding plasma, ionizing additional neutrals in route to the substrate [11]. In the presented work, the work carried out by Raman et al. [9,10] is continued for a linear magnetron. A high deposition rate, scalable linear magnetron magnet pack is modeled and experimentally tested.

2. Materials and methods

When DC magnetron sputtering is mentioned, the DC power supply used is the Advanced Energy Pinnacle Series DC Magnetron Power Supply with a 20 kW power limit, a 50 A average current limit and a 1 kV average voltage limit. When HiPIMS is mentioned, the power supply used is a Huttinger TruPlasma 4002 HiPIMS power supply capable of up to 10 kW average power, voltages up to 2 kV, currents up to 1 kA, frequencies up to 500 Hz, and pulse lengths up to 200 microseconds. A 12.7 × 25.4 cm^2 Lesker magnetron is used for all testing.

* Corresponding author.
E-mail address: jmclain2@illinois.edu (J. McLain).

https://doi.org/10.1016/j.vacuum.2018.06.023
Received 24 April 2018; Received in revised form 7 June 2018; Accepted 8 June 2018
Available online 15 June 2018
0042-207X/

Deposition rate tests were performed by placing 20 samples in front of one quadrant of the sputtering target at a distance of 10 cm away from the target surface. Each sample is a 2.54 cm 316 stainless steel circle substrate, where the deposition rate is determined through mass change. The mass change deposition rate method was validated by comparing against both profilometry and a quartz crystal microbalance.

A triple Langmuir probe is used to measure the electron densities and temperatures throughout the pulse. This pulsed plasma diagnostic has been used for many pulsed plasma applications in the past and the physics is well studied [12–15]. There are various contributors to the error in these measurements. These factors include the assumption of a non-magnetic plasma, the assumption of a Maxwellian electron distribution, and using a metal deposition chamber, which inherently deposits on the probes. After the initial spike in the electron temperature, the plasma quickly becomes Maxwellian, which is seen after 50 microseconds, and the assumption of a non-magnetic plasma holds true at the substrate, 10.2 cm from the target, but may not at the target, 1.3 cm from the target. It is also important to note that the temperatures are approximate temperatures based on triple Langmuir probe theory.

A final experiment that was carried out was the measurement of the ionized flux fraction at the substrate, 10.2 cm from the target surface. A diagnostic used to determine the fraction of ions vs. total target atoms to the substrate is the gridded energy analyzer-QCM tool (GEA) as described in K. M. Green et al. [16], named the GEA. When working in iPVD systems, careful design considerations must be taken and have been established in Meng et al. and Wu [17,18]. The top grid is exposed to the floating potential of the plasma and has the role of stopping plasma penetration into the device. Then the middle grid is biased to a sufficiently high negative potential as to repel the high energy electrons. Lastly, the bottom grid has the role of either attracting or repelling ions. Under the triple grid setup, there is a QCM, used to measure the deposition rate of metal atoms that pass through the grids.

To repel ions, the bottom grid is biased to a sufficiently high positive potential, and to attract all ions, the bottom grid is biased to a sufficiently high negative potential. With the neutral atom deposition rate and the ion plus neutral deposition rate known, the ionized flux fraction can be simply calculated. To determine what is considered sufficient, a voltage sweep is carried out and deposition rate recorded. At the negative end and at the positive end, the deposition rate eventually reaches a maximum or a minimum. At those voltages, the voltage applied is considered sufficiently high.

2.1. Theory and modeling

The magnetic field strength allows for confinement of electrons, necessary for basic operation of a magnetron, and the shape of the fields not only helps with confinement, but also dictates the path that electrons travel. The proposed design of a new linear magnet pack, called the linear tripack magnet pack, has three zones of electron confinement with magnetic fields that allow for controlled loss of electrons in order to increase deposition rate of ions, previously shown and explained in Raman et al. [11] The linear tripack magnet pack has high field regions over each of the racetracks, which allow for basic magnetron operation, but these high field regions fall off 90% in magnitude, less than 2 cm from the target surface, allowing for electrons to travel along open field lines created by neighboring, opposite direction magnetic field lines. This is seen in Fig. 1a. These electrons escape the magnetic field trap and cause an ambipolar field that forces the ions out of the electric field that causes much of the return effect. This allows for a plasma that expands toward the substrate, increasing ionizations. As shown in Fig. 1b, a standard magnet pack magnetic field extends much further, causing a stronger electron trap and return effect, reducing deposition rate. COMSOL Multiphysics finite element software was used for all of the modeling. Fig. 1a shows a 2D cross section of the tripack magnet pack magnetron with associated magnetic fields and strengths. The zero point on the width of the figure is on the edge of the target. A positive

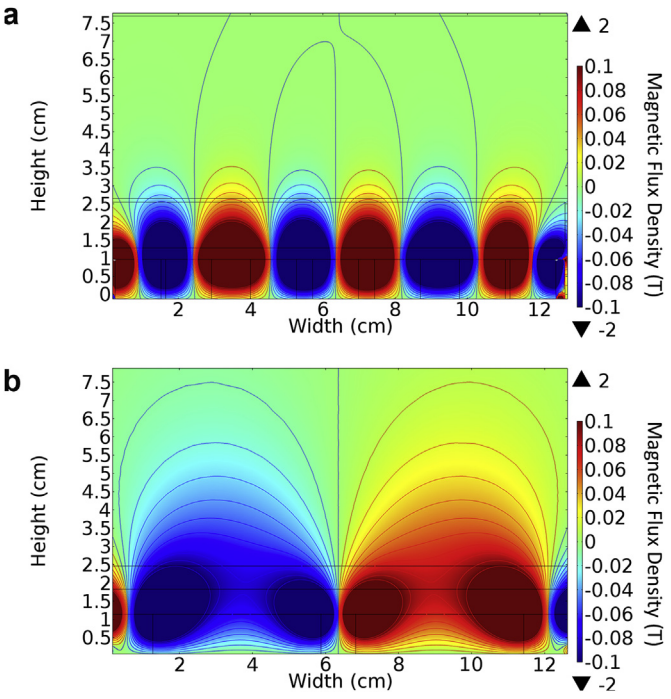

Fig. 1. (A) (Color Online) 2D cross sectional view of the linear tripack magnet pack magnetic field and magnitude. (b) 2D cross sectional view of the linear conventional magnet pack magnetic field and magnitude. (For interpretation of the references to colour in this figure legend, the reader is referred to the Web version of this article.)

value corresponds to a field oriented towards the right, and a negative value corresponds to a field oriented to the left. The black line at a height of 2.54 cm is the target surface. In Fig. 1a and b, the other black lines are simply boundaries for different mesh densities in the simulation.

Fig. 1a shows that the tripack magnet pack has closed field lines around each of the confinement regions, but also has regions between neighboring field lines for controlled loss of electrons. The magnetic field magnitude parallel to the target at the surface of the magnet pack is seen in Fig. 2. This figure shows that the maximum and minimum values at the target are about 0.067 T and 0.045 T, respectively. The simulated maximum and minimum magnetic field strength in a standard commercial magnet pack are experimentally measured and confirmed.

The final step that is taken in the modeling is to see how electrons behave in the magnetic field configuration. This simulation is simply a proof of concept and a visual aid, as opposed to a quantitative study. 2D and 3D COMSOL Multiphysics modeling of the electron trajectories is carried out. The assumptions made are 0.13 Pa (1 mTorr) Argon electron-neutral collisions, electron-electron coulombic collisions, a −600 V target bias, and 1000 electrons released at 1eV normal to the target surface, along half of the target's centerline. The black box in Fig. 2 shows the region where the electrons are ejected for the simulation.

The three confinement regions had electrons traveling in the ExB direction and there were some electrons that made their way out of the erosion zones. Because the electrons are confined for the entire confinement region, the magnetron can operate normally. More importantly, because there is some controlled electron loss by increasing the cross-field diffusion, the driving mechanism behind the increased deposition rate still holds due to the ambipolar electric field created by the charge separation between the escaping electrons and trapped ions. This can also be explained as with an increase in the electron diffusion coefficient comes an increased ambipolar diffusion coefficient over the

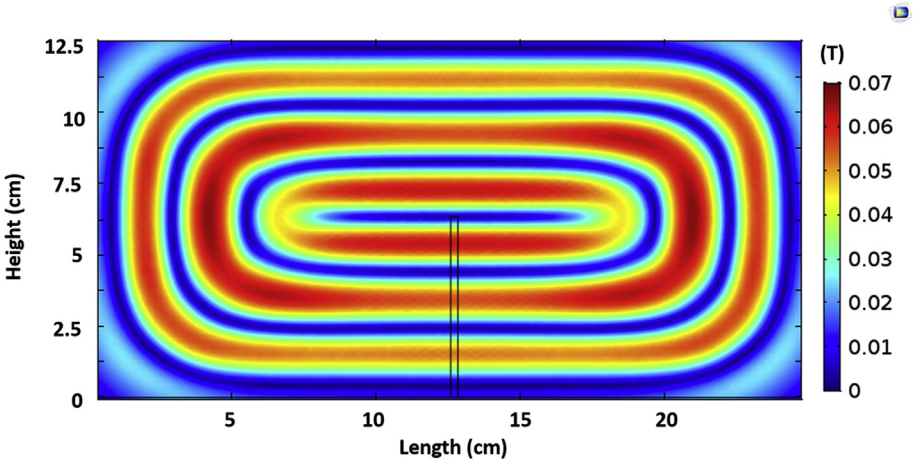

Fig. 2. (Color Online) 2D cross section of the magnetic field magnitude on the target surface of the linear tripack magnet pack. (For interpretation of the references to colour in this figure legend, the reader is referred to the Web version of this article.)

standard magnet pack, as shown in the modeling by Raman et al. [11]. This allows for ambipolar diffusion of ions out of the magnetic trap near the target, toward the substrate.

To better visualize this and confirm that there is cross field diffusion, a 2D simulation was run along the centerline width of the magnetron and confirmed that there was an increase in diffusion across the magnetic field lines when compared with the conventional magnet pack, as seen in Fig. 3a and b. The figure only shows up to 50 eV for scaling purposes, though the expected 600 eV is seen early in the simulation. The principle on which this magnet pack is designed, is that manipulating magnetic fields to allow for more electrons to escape the magnetic trap will allow for charge separation and an ambipolar field to be created that will force more ions to leave the high electric field trap and create an expanding plasma that increases ionizations of sputtered material, hence increasing deposition rate. Essentially, this method reduces the effect of recycling ionized target material. These modeling results lead to the physical creation of the linear tripack magnet pack, and the experimental results are discussed in the following section.

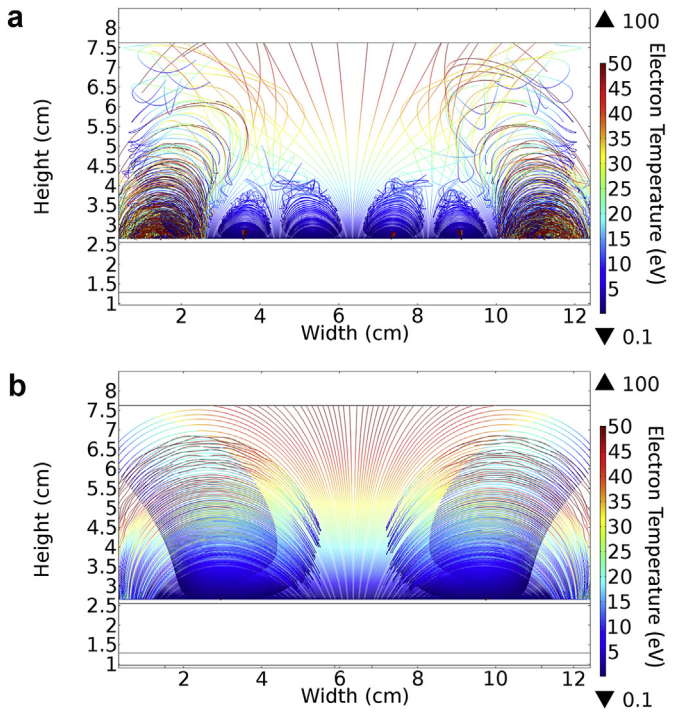

Fig. 3. (A) (Color Online) 2D particle tracing simulation for the linear tripack magnet pack. (b) 2D particle tracing simulation for the linear conventional pack. (For interpretation of the references to colour in this figure legend, the reader is referred to the Web version of this article.)

3. Results and discussion

3.1. Magnetron operation

The linear tripack magnet pack was built according to the magnetic specifications determined by the model. A comparison between the I-V curves for the standard magnet pack and the linear tripack magnet pack is seen in Fig. 4. A confinement parameter of n = 6 is seen for the standard magnet pack, which is within the typical range [19]. The linear tripack has a confinement parameter of n = 3, which is less than a standard magnetron magnet pack, which is a desired trait for this design, as more escaping electrons from the magnetic trap is desired. It is seen that the transition to the HiPIMS mode occurs for both magnet packs, and the current quickly increases with voltage due to the trapping of ions in the magnetic trap. At the high end of the I-V curves, there is a current limitation do to the power supply average current limit.

The HiPIMS voltage and current traces for the linear tripack and

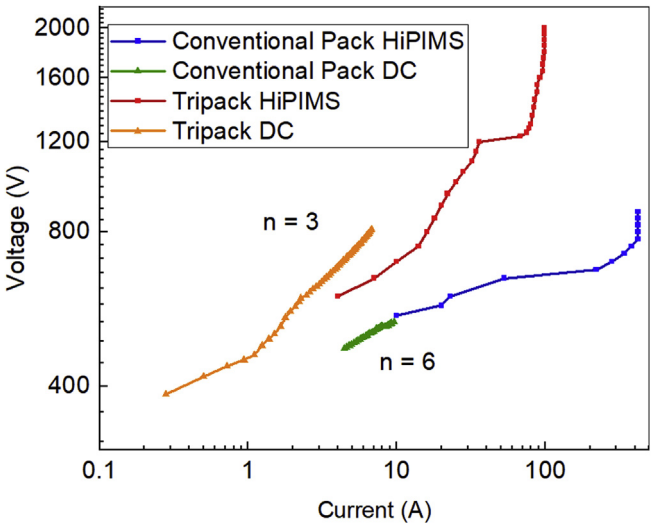

Fig. 4. (Color Online) Standard and linear tripack magnet pack I-V curves. (For interpretation of the references to colour in this figure legend, the reader is referred to the Web version of this article.)

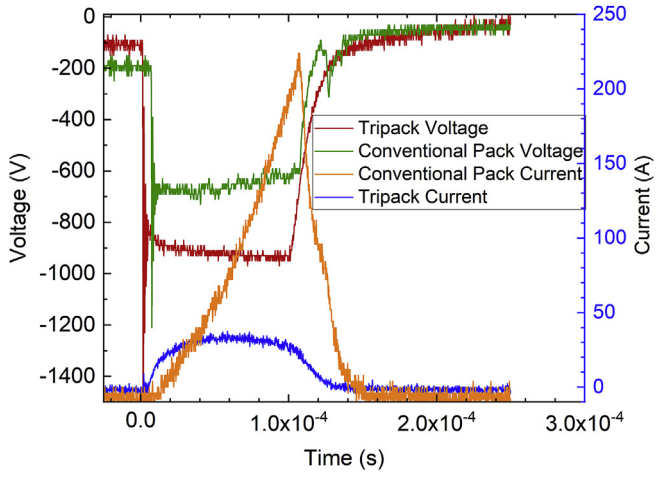

Fig. 5. (Color Online) Voltage and current waveforms for the conventional and tripack magnet packs. The operating pressure is 0.67 Pa (5 mTorr) of argon at 1.5 kW average power with a copper target using the Huttinger TruPlasma 4002 HiPIMS power supply. (For interpretation of the references to colour in this figure legend, the reader is referred to the Web version of this article.)

standard magnet pack are compared in Fig. 5. Both magnet packs were operated with new copper targets at a 1.5 kW average power. Target erosion was less than 1% of total target thickness during all experiments. The conventional magnet pack has a peak current of 225 A, whereas the linear tripack magnet pack has a peak current of 35 A. At 1.5 kW in DCMS, the tripack has a current of 3.3 A, and the standard magnet pack has a current of 2.5 A. The decrease in current is due to the decrease in sputtered ions returning to the target.

The voltage and current waveforms for the tripack and standard magnet pack in HIPIMS are seen in Fig. 5. Voltage is measured between the HiPIMS power supply and the magnetron target using a 100:1 voltage probe. Current is measured at the same location as the voltage using a Rogowski probe. Time is zero at the beginning of the pulse. Ideally, the pulse width and frequency would be constant across magnet packs, but in the case of the conventional magnet pack, frequency needed to be adjusted for arc control and power control. The average power and pulse width between the two magnet packs was constant, but the frequency varied up to 10%. The power supply always began the pulse at a negative voltage, regardless of the magnet pack. There is a qualitative observation that many fewer arcs are seen when using the tripack magnet pack when compared with the conventional magnet pack. These observations will be quantified in future work.

3.2. Deposition rate

Fig. 6 shows the deposition rate across the center-line length of a 12.7 by 25.4 cm copper target, where length is measured from the edge of the target. Operation is at 0.67 Pa (5 mTorr) argon at 1.5 kW average power for both DCMS and HiPIMS. Average power is calculated by integrating the product of the voltage and current waveforms from the diagnostic probes and multiplying by the operating frequency. Fig. 7 displays the deposition rate across the center-line width of the copper target for the same conditions as in Fig. 6. Note that the data was taken across half of the target and mirrored onto the other half for visual simplicity, which can be done due to symmetry.

Figs. 6 and 7 show that the HiPIMS tripack produced deposition rates that were equal to those produced by conventional magnet pack DC across the center-line width of the target, and greater than conventional magnet pack DC across the centerline length of the target. The tripack operated in HiPIMS produced the highest deposition rates across both tested magnet packs and power supplies at 1.5 kW. A 3.2 kW experiment was also carried out. For this power, the tripack

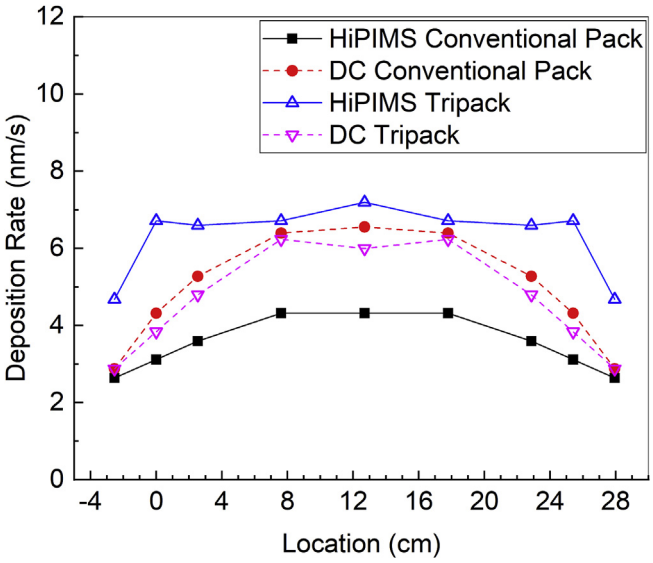

Fig. 6. (Color Online) 1.5 kW Copper deposition rates across the centerline length of the target with 0.67 Pa (5 mTorr) argon at the substrate, 10.2 cm away from the target. (For interpretation of the references to colour in this figure legend, the reader is referred to the Web version of this article.)

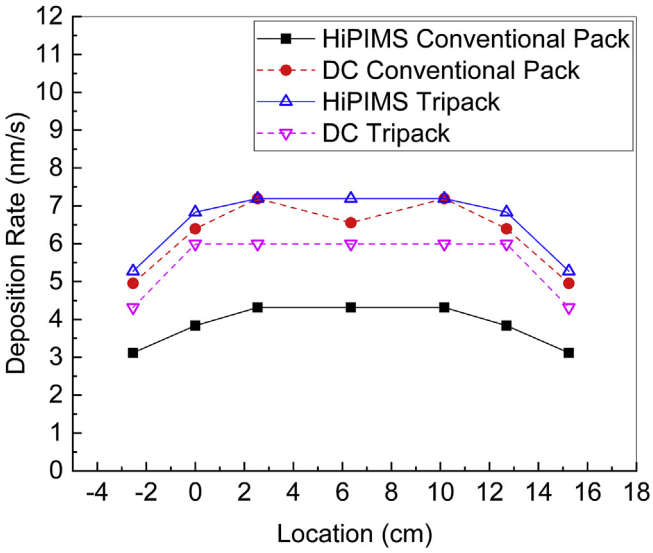

Fig. 7. (Color Online) 1.5 kW Copper deposition rates across the centerline width of the target with 0.67 Pa (5 mTorr) argon at the substrate, 10.2 cm away from the target. (For interpretation of the references to colour in this figure legend, the reader is referred to the Web version of this article.)

HiPIMS deposition rate was lower the conventional DC, but it was greater than the conventional magnet pack HiPIMS deposition rate by 25%.

At higher powers, the DCMS deposition rate is higher than the HiPIMS deposition rate. The key finding however, is that the HiPIMS deposition rate with the tripack is significantly higher than the HiPIMS deposition rate with the standard magnet pack. Also, as the power is raised, the voltage must increase. Our weakened magnetic trap pushes the ionization zone higher above the target, deeper in to the pre-sheath. As the voltage is raised, the voltage difference for ions to escape is also increased, causing the magnetic trap manipulation to become less effective.

Pushing the ionization zone further from the target essentially allows for an ionization region without the negative effects of the electric and magnetic trap that hinders deposition rate in HiPIMS discharges.

This expanding plasma region is due to the tripack's stronger magnetic field gradient traveling away from the target. This gradient allows for a larger electron Larmor radius closer to the target when compared with the standard magnet pack, leading to an increase in the electron diffusion coefficient across magnetic field lines, and therefore an increased ambipolar diffusion coefficient when compared to the standard magnet pack. A complete derivation of the increase in ambipolar diffusion coefficient is found in Raman et al. [11]. This is the driving mechanism behind the increased deposition rate in the HiPIMS tripack magnet pack over a standard HiPIMS magnet pack.

We assume that our ions are singly ionized. If the ions had a higher degree of ionization, a larger energy ion would be needed to escape this trap, which would lead to a decrease in deposition rate. It is also seen that the uniformity is better for the tripack magnet pack, when compared with the conventional magnet pack, which can also lead to an increase in target utilization. The deposition rate and modeling results suggest that an increased number of electrons, and therefore ions, escape the magnet trap. Triple Langmuir probe diagnostics were carried out to test this theory at the substrate, 10 cm away from the target.

The electron temperature was measured using a 45 V bias, so any measurement that is over 30 eV has increasing error associated with it because the voltage bias on the probe must be much larger than the temperature. The density calculation depends on the temperature as $Te^{1/2}$. Above 30 eV, no data should be considered a quantitative measurement, but should be only treated as a trend observed in the pulse. At this point in the trace, the density is very low because only the high energy tail has reached the probe at the substrate, 10 cm away. During the pulse, it is seen that the density is increasing, and the temperature is decreasing. This is expected because the lower energy electrons then reach the probe and more collisions occur, bringing down the electron temperature. At the end of the pulse, an equilibrium is seen in the density and temperature, where the density is about 1.7×10^{19} m-3, and the temperature is between 1 and 2 eV, where similar values are reported in Gudmundsson et al. [20].

A calculation of the fraction of copper ionized en route to the substrate can be seen in equation (1). The electron density (n_e) is measured and the cross section (σ_{e-Cu}) [21] for the electron impact ionization of copper can be found during the pulse, at the substrate. The calculation assumes our expanding plasma is 7.5 cm in length (l_{plasma}) with our substrate 10 cm from the target, our frequency (f) is 400 Hz, and our Cu atoms sputter at 1.77eV [22]. The electron temperature is measured allowing for the velocity (v_e) to be calculated and the copper sputtering energy allows for the copper velocity (v_{Cu}) to be calculated. The ionized flux fraction calculation is integrated over the pulse time and suggests that 6% of sputtered copper atoms are ionized en route to the substrate via the expanding plasma using the tripack in HiPIMS at 3200 W. Fig. 8 shows this calculation of ionized flux fraction of sputtered copper atoms at 1.5 kW for the tripack and conventional pack in HiPIMS and DC. These measurements support that the tripack magnet pack creates ionizations en route to the substrate.

In previous work, the ionized flux fraction, defined as delta, had values somewhat larger (15%), but that was for a different magnet pack and magnetron set-up [11,23]. Note that ionization of sputtered atoms is a secondary source of ionized target atoms. There is still the group of sputtered neutral atoms which is ionized by the intense plasma adjacent to the target itself, as in HIPIMS with standard magnet packs.

Ionized flux fraction of Copper Atoms Within the Expanding Plasma

$$= \frac{\int_{0\,s}^{200\,\mu s} n_e n_{Cu} \sigma_{e-Cu} v_e dt * fl_{plasma}}{v_{Cu} n_{Cu}} \quad (1)$$

Fig. 9 shows the electron density profiles for both the conventional and tripack magnet packs for 1.5 kW. We see that a higher density, steady profile is seen at the substrate, 10.2 cm away from the magnetron for the linear tripack magnet pack. The standard magnet pack on the other hand, has a peak density that is reached for a short period of time. Fig. 10 shows the peak electron densities at the substrate at 1.5 kW, and Fig. 12 shows the peak electron densities at the target at 1.5 kW. Figs. 12 and 14 show the peak temperatures at the substrate and target. It should be noted that the triple Langmuir probe theory gives an approximate energy for a given time. The magnetic field arrangement of the tripack magnet pack is designed to allow for an expanding plasma to increase ionizations in route to the substrate, as is discussed in Raman et al. [11]. The electron density at the target is about the same for the conventional and tripack magnet pack, keeping the general operation of the magnetron from changing, but there is a notable qualitative decrease in arcing with the tripack magnet pack, suggesting a decrease in hotspot formation [24]. It is also important to note that the triple Langmuir probe is affected by magnetic field lines, which could result in error in the near target region. The electron density at the substrate on the other hand, is about an order of magnitude higher for the tripack magnet pack than for the conventional magnet pack. This is consistent with the theory that an expanding plasma can increase ionizations en route to the substrate.

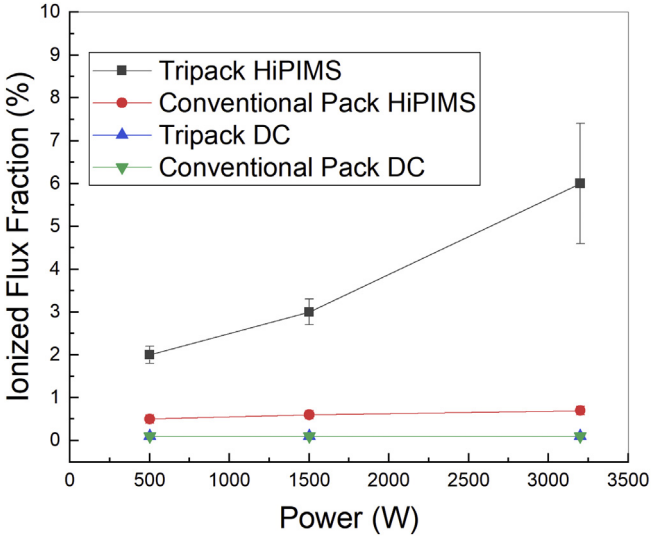

Fig. 8. (Color Online) Expanding Plasma Ionized flux fraction for the Tripack and Conventional Pack. (For interpretation of the references to colour in this figure legend, the reader is referred to the Web version of this article.)

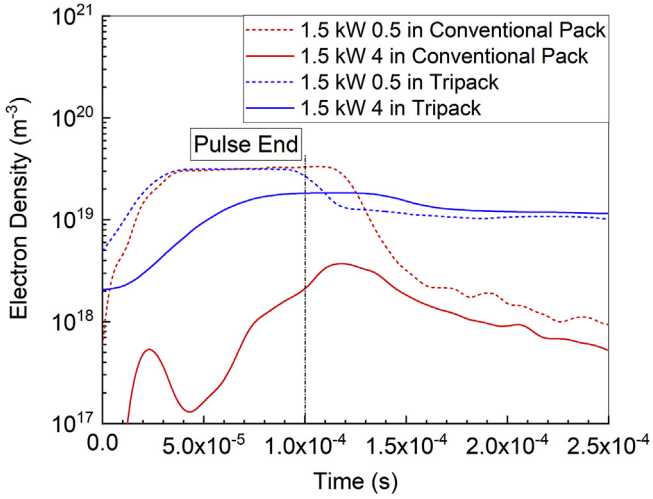

Fig. 9. (Color Online) Electron density profiles for 1.5 kW average power at the target, 1.27 cm away from the target surface, and at the substrate, 10.2 cm away from the target surface, where the pulse begins at 0 s and the pulse ends at 100 microseconds. (For interpretation of the references to colour in this figure legend, the reader is referred to the Web version of this article.)

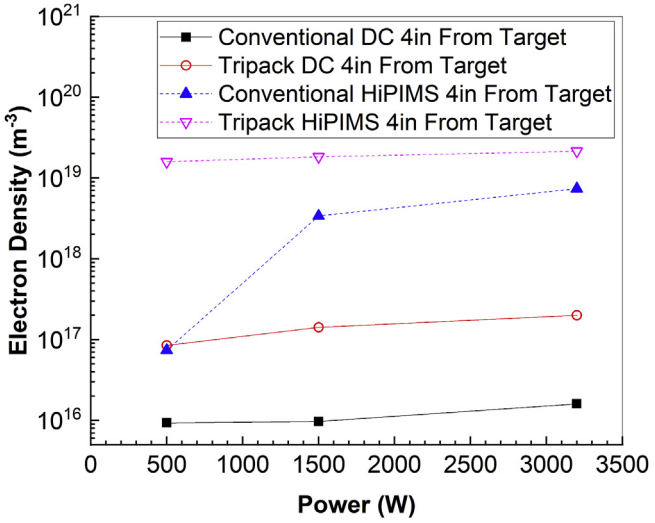

Fig. 10. (Color Online) Peak electron densities at the substrate, 10.2 cm from the target surface, across different powers. (For interpretation of the references to colour in this figure legend, the reader is referred to the Web version of this article.)

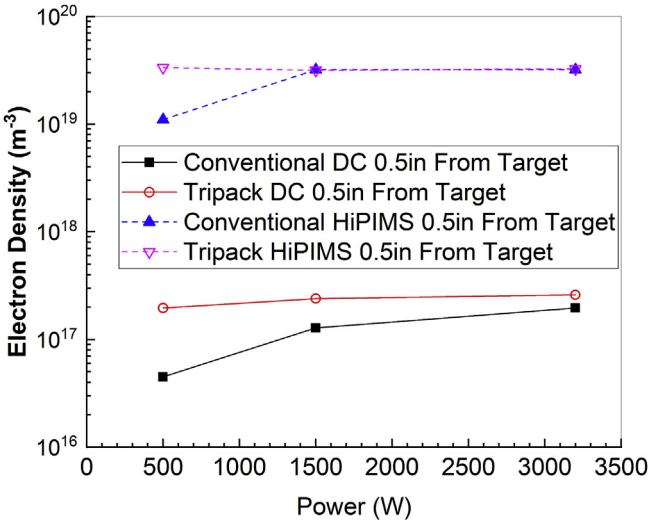

Fig. 12. (Color Online) Peak electron densities at the target, 1.27 cm from the target surface, across different powers. (For interpretation of the references to colour in this figure legend, the reader is referred to the Web version of this article.)

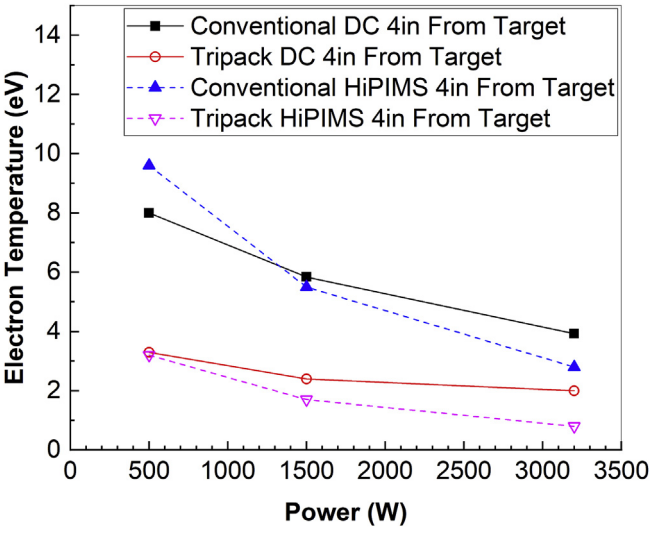

Fig. 11. (Color Online) Peak electron temperature at the substrate, 10.2 cm from the target surface, across different powers. (For interpretation of the references to colour in this figure legend, the reader is referred to the Web version of this article.)

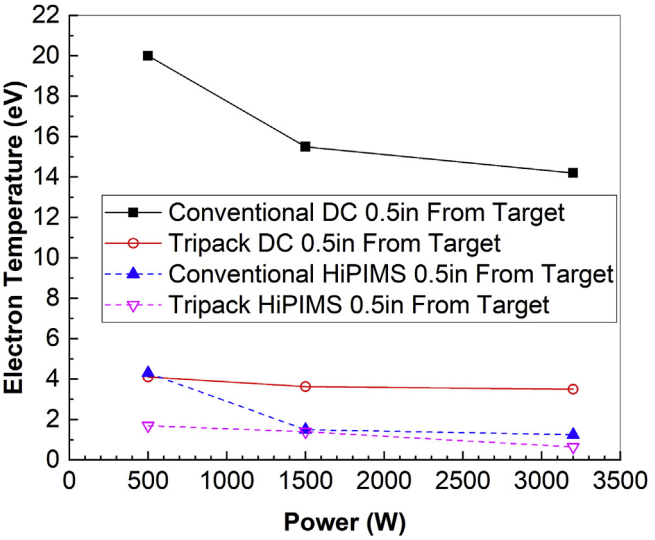

Fig. 13. (Color Online) Peak electron temperature at the target, 1.27 cm from the target surface, across different powers. (For interpretation of the references to colour in this figure legend, the reader is referred to the Web version of this article.)

The peak densities in the near target, highly confined plasma are about the same for both magnet packs used in HiPIMS. The densities at the substrate, on the other hand, are not equal. There is about a factor of three difference between the tripack and standard magnet pack at 1.5 kW in HiPIMS mode. There is also an order of magnitude difference between the tripack and standard pack in DC mode. These two comparisons experimentally show that there is a definite increase in electron loss when using the tripack magnet pack, which again suggests an increase of deposition rate by ambipolar diffusion.

Fig. 14 shows the ionized flux fraction for the tripack and standard magnet pack for DC and HiPIMS. This data was taken using a gridded energy analyzer. It is seen that the ionized flux fraction to the substrate is greater for HiPIMS than for DC, as expected, but it also shows that for DC and HiPIMS, the ionized flux fraction is greater when using the tripack magnet pack over the standard magnet pack. We again assume that the ions being measured are singly ionized, which indicates that a simple calculation can be made for ionized flux to the target, when deposition rate is known. Raman et al. found an ionized flux fraction of 16% for a 4 inch magnetron [11]. Meng et al. measured an ionized flux fraction of 16% for 800G and 19% for 500G at the target at −1100 V on the target [1]. The results for the linear tripack magnet pack was measured to have an ionized flux fraction of 21% at 1500 W and −1200 V, agreeing very well with these sources that use the same diagnostic method. The benefit of the linear tripack magnet is its ability to scale power higher than the literature, allowing for an increased ionized flux fraction. This is an additional reassurance that there is indeed a higher ion flux to the substrate that is consistent with the ionizations in route to the substrate theory established by Raman et al. [11]. The conclusion that the ion flux is higher is derived in part that the tripack magnet pack has a higher deposition rate than the standard magnet pack, which was discussed in Figs. 6 and 7.

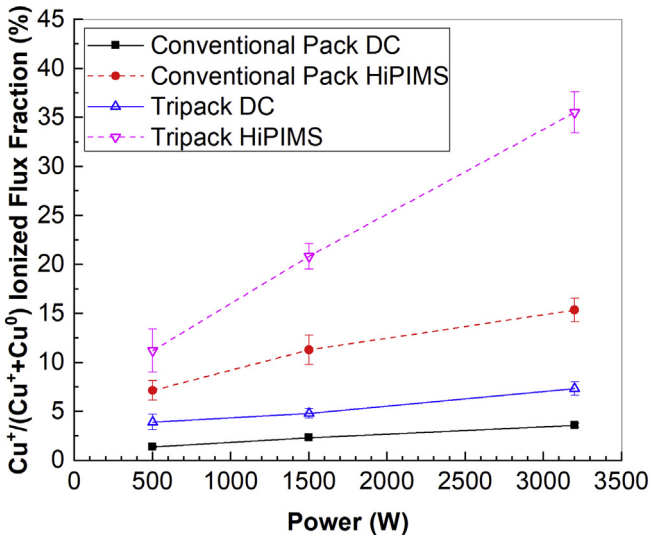

Fig. 14. (Color Online) Ionized flux fraction measurements at the substrate, 10.2 cm from the target surface, for DCMS and HiPIMS with the standard magnet pack and tripack. (For interpretation of the references to colour in this figure legend, the reader is referred to the Web version of this article.)

4. Conclusions

The tripack magnet pack was designed and built with the intension of confining electrons for proper magnetron operation, but also allowing an increased number of electrons to escape the magnetic trap. The additional escaping electrons allow for an increased deposition rate by pulling ions out of the magnetic and electric trap by ambipolar diffusion and also allow for an expanding plasma toward the substrate. This expanding plasma gives rise to an increased ionized flux fraction measured at the substrate. The modeling suggested an increased electron loss, the I-V curve for the tripack showed a decreased confinement parameter value when compared with the standard magnet pack, and the electron density at the substrate increased when compared with the standard magnet pack. These results all agree that the tripack allows for an increased loss of electrons. The deposition rate results all show an increased tripack deposition rate in HiPIMS mode when compared with the standard magnet pack. The magnetic field topology allowed for the increased electron flux away from the target and also the increased deposition rate of copper, and copper ions to the substrate. The number of arcs on the target surface also decreased by more than an order of magnitude during testing when using the linear tripack.

Acknowledgements

This research was funded by the NSF Center for Lasers and Plasmas for Advanced Manufacturing, award number 0934400. Funding was also provided by the NSF Accelerating Innovation Research – Technology Translation Program, award number 1500271, and the NSF Industry-University Cooperative Research Centers Program, award number 1540030. This work was carried out partially at the Beckman Institute Imaging Technology group and the University of Illinois at Urbana Champaign.

References

[1] Liang Meng, He Yu, Matthew M. Szott, Jake T. McLain, David N. Ruzic, J. Appl. Phys. 115 (2014) 223301, http://dx.doi.org/10.1063/1.4878622.
[2] Ulf Helmersson, Martina Lattemann, Johan Bohlmark, Arutiun P. Ehiasarian, Jon Tomas Gudmundsson, Thin Solid Films 513 (2006) 1.
[3] M. Samuelsson, D. Lundin, J. Jensen, M.A. Raadu, J. Gudmundsson, U. Helmersson, Surf. Coating. Technol. 205 (2010) 591–596.
[4] He Yu, Liang Meng, Matthew M. Szott, Jake T. McLain, Tae S. Cho, David N. Ruzic, Plasma Sources Sci. Technol. 22 (4) (2013) 045012.
[5] U. Helmersson, M. Lattemann, J. Alami, J. Bohlmark, A.P. Ehiasarian, J.T. Gudmundsson, Proceedings of the 48th Annual Technical Conference of the Society of Vacuum Coaters, April 23–28, 2005, Denver, CO, USA, 2005, p. 458.
[6] S. Konstantinidis, J.P. Dauchot, M. Ganciu, a Ricard, M. Hecq, J. Appl. Phys. 99 (2006) 13307.
[7] J. Capec, M. Hala, O. Zabeida, J.E. Klemberg-Sapieha, L. Martinu, J. Appl. Phys. 46 (2013) 205205.
[8] Anurag Mishra, P.J. Kelly, J.E. Bradley, Plasma Sources Sci. Technol. 19 (2010) 045014.
[9] Priya Raman, Ivan Shchelkanov, Jake McLain, Matthew Cheng, David Ruzic, Ian Haehnlein, Brian Jurczyk, Robert Stubbers, Sean Armstrong, Surf. Coating. Technol. 293 (15) (May 2016) 10–15.
[10] Priya Raman, Ivan A. Shchelkanov, Jake McLain, David N. Ruzic, J. Vac. Sci. Technol. A (2015) 33 031304.
[11] Priya Raman, Justin Weberski, Matthew Cheng, Ivan Shchelkanov, David N. Ruzic, J. Appl. Phys. 120 (2016) 163301.
[12] Liang Meng, A.N. Cloud, S. Jung, D.N. Ruzic, J. Vac. Sci. Technol. A (2011) 29 011024.
[13] Soonwook Jung, Daniel Andruczyk, D.N. Ruzic, IEEE Trans. Plasma Sci. 40 (3) (2012) 730–734.
[14] S.L. Chen, T. Sekiguchi, J. Appl. Phys. 36 (8) (1965) 2363–2375.
[15] C. Riccardi, G. Longoni, G. Chiodini, M. Fontanesi, Rev. Sci. Instrum. 72 (1) (2001) 461–464.
[16] K.M. Green, D.B. Hayden, D.R. Juliano, D.N. Ruzic, Rev. Sci. Instrum. 68 (12) (1997) 4555–4560.
[17] Liang Meng, Ramasamy Raju, Randolph Flauta, Hyungjoo Shin, David N. Ruzic, Douglas B. Hayden, J. Vac. Sci. Technol. A 28 (1) (2010) 112–118.
[18] YuiLun Wu, Diagnostics for Ionized Physical Vaport Deposition chambers, PhD Dissertation (2016).
[19] J.A. Thornton, J. Vac. Sci. Technol 15 (2) (1978) 171–177.
[20] J.T. Gudmundsson, P. Sigurjonsson, P. Larsson, D. Lundin, U. Helmersson, J. Appl. Phys. 105 (2009) 123302.
[21] Philip L. Bartlett, Andris T. Stelbovics, The American Physical Society, (2002), p. 66 012707.
[22] Michael A. Lieberman, Allan J. Lichtenberg, Chemical Kinetics and Surface Processes", Principles of Plasma Discharges and Materials Processing, 308, Wiley, Hoboken, New Jersey, 2005.
[23] Jake McLain, Linear Magnetron High Deposition Rate Magnet Pack for High Power Impulse Magnetron Sputtering, Master's Thesis (2016).
[24] Raman, et al., Stabilization of Ionization Zones in High Power Impulse Magnetron Sputtering, Vacuum (2018) In Review.